J|A|C|S ARTICLES

Published on Web 12/23/2008

Layer-by-Layer Assembly of All Carbon Nanotube Ultrathin Films for Electrochemical Applications

Seung Woo Lee,[†,||] Byeong-Su Kim,[†] Shuo Chen,[‡,||] Yang Shao-Horn,[*,‡,§,||] and Paula T. Hammond[*,†]

Department of Chemical Engineering, Department of Mechanical Engineering, Department of Materials Science and Engineering, and Electrochemical Energy Laboratory, Massachusetts Institute of Technology, Cambridge, Massachusetts 02139

Received September 5, 2008; E-mail: shaohorn@mit.edu; hammond@mit.edu

Abstract: All multiwall carbon nanotube (MWNT) thin films are created by layer-by-layer (LBL) assembly of surface functionalized MWNTs. Negatively and positively charged MWNTs were prepared by surface functionalization, allowing the incorporation of MWNTs into highly tunable thin films via the LBL technique. The pH dependent surface charge on the MWNTs gives this system the unique characteristics of LBL assembly of weak polyelectrolytes, controlling thickness and morphology with assembly pH conditions. We demonstrate that these MWNT thin films have randomly oriented interpenetrating network structure with well developed nanopores using AFM and SEM, which is an ideal structure of functional materials for various applications. In particular, electrochemical measurements of these all-MWNT thin film electrodes show high electronic conductivity in comparison with polymer composites with single wall nanotubes, and high capacitive behavior with precise control of capacity.

Introduction

Carbon nanotubes (CNT) are some of the most promising materials for the design of functional thin films, including those for catalytic membranes,[1,2] actuation,[3,4] and mechanical thin film applications,[5] and perhaps most importantly for a range of electrochemical energy conversion and storage devices (such as fuel cells,[6−8] batteries,[9−11] and supercapacitors[12−14]), due to their unique physical properties, including high electrical conductivity, superior chemical and mechanical stability, and large surface area.[15,16] Controlling the architecture of CNT thin films at the nanometer and micrometer-scale is critical to tailoring film properties and functionality.[17] For example, functional films of CNTs with vertically oriented geometries have been prepared using vapor deposition[12,18,19] and filtration,[20] but it is difficult to make dense films with low porosity with these methods. Nanocomposites with polymer have been developed,[4,21] but limitations exist in the processibility of CNTs in solution, as CNTs precipitate into ropes or bundles due to strong van der Waals interactions between CNTs. Various surface modifications of CNTs have been employed to disperse CNTs, including chemical functionalization using strong acids,[22,23]

[†] Department of Chemical Engineering.
[||] Electrochemical Energy Laboratory.
[‡] Department of Mechanical Engineering.
[§] Department of Materials Science and Engineering.

(1) Holt, J. K.; Park, H. G.; Wang, Y. M.; Stadermann, M.; Artyukhin, A. B.; Grigoropoulos, C. P.; Noy, A.; Bakajin, O. *Science* **2006**, *312*, 1034–1037.
(2) Smajda, R.; Kukovecz, A.; Konya, Z.; Kiricsi, I. *Carbon* **2007**, *45*, 1176–1184.
(3) Baughman, R. H.; Cui, C. X.; Zakhidov, A. A.; Iqbal, Z.; Barisci, J. N.; Spinks, G. M.; Wallace, G. G.; Mazzoldi, A.; De Rossi, D.; Rinzler, A. G.; Jaschinski, O.; Roth, S.; Kertesz, M. *Science* **1999**, *284*, 1340–1344.
(4) Landi, B. J.; Raffaelle, R. P.; Heben, M. J.; Alleman, J. L.; VanDerveer, W.; Gennett, T. *Nano Letters* **2002**, *2*, 1329–1332.
(5) Mamedov, A. A.; Kotov, N. A.; Prato, M.; Guldi, D. M.; Wicksted, J. P.; Hirsch, A. *Nat. Mater.* **2002**, *1*, 190–194.
(6) Wang, C.; Waje, M.; Wang, X.; Tang, J. M.; Haddon, R. C.; Yan, Y. S. *Nano Lett.* **2004**, *4*, 345–348.
(7) Michel, M.; Taylor, A.; Sekol, R.; Podsiadlo, P.; Ho, P.; Kotov, N.; Thompson, L. *Adv. Mater.* **2007**, *19*, 3859–3864.
(8) Li, W. Z.; Liang, C. H.; Zhou, W. J.; Qiu, J. S.; Zhou, Z. H.; Sun, G. Q.; Xin, Q. *J. Phys. Chem. B* **2003**, *107*, 6292–6299.
(9) Frackowiak, E.; Gautier, S.; Gaucher, H.; Bonnamy, S.; Beguin, F. *Carbon* **1999**, *37*, 61–69.
(10) Shimoda, H.; Gao, B.; Tang, X. P.; Kleinhammes, A.; Fleming, L.; Wu, Y.; Zhou, O. *Phys. Rev. Lett.* **2002**, *88*, 015502.
(11) Morris, R. S.; Dixon, B. G.; Gennett, T.; Raffaelle, R.; Heben, M. J. *J. Power Sources* **2004**, *138*, 277–280.
(12) Futaba, D. N.; Hata, K.; Yamada, T.; Hiraoka, T.; Hayamizu, Y.; Kakudate, Y.; Tanaike, O.; Hatori, H.; Yumura, M.; Iijima, S. *Nat. Mater.* **2006**, *5*, 987–994.
(13) Yoon, B. J.; Jeong, S. H.; Lee, K. H.; Kim, H. S.; Park, C. G.; Han, J. H. *Chem. Phys. Lett.* **2004**, *388*, 170–174.
(14) Frackowiak, E.; Beguin, F. *Carbon* **2001**, *39*, 937–950.
(15) Baughman, R. H.; Zakhidov, A. A.; de Heer, W. A. *Science* **2002**, *297*, 787–792.
(16) Ajayan, P. M.; Zhou, O. Z. In *Carbon Nanotubes*; Springer-Verlag: Berlin, 2001; Vol. 80, pp 391−425.
(17) Arico, A. S.; Bruce, P.; Scrosati, B.; Tarascon, J. M.; Van Schalkwijk, W. *Nat. Mater.* **2005**, *4*, 366–377.
(18) Shaijumon, M. M.; Ou, F. S.; Ci, L. J.; Ajayan, P. M. *Chem. Commun.* **2008**, 2373–2375.
(19) Pushparaj, V. L.; Shaijumon, M. M.; Kumar, A.; Murugesan, S.; Ci, L.; Vajtai, R.; Linhardt, R. J.; Nalamasu, O.; Ajayan, P. M. *Proc. Natl. Acad. Sci. U.S.A.* **2007**, *104*, 13574–13577.
(20) Li, W. Z.; Wang, X.; Chen, Z. W.; Waje, M.; Yan, Y. S. *Langmuir* **2005**, *21*, 9386–9389.
(21) An, K. H.; Jeon, K. K.; Heo, J. K.; Lim, S. C.; Bae, D. J.; Lee, Y. H. *J. Electrochem. Soc.* **2002**, *149*, A1058–A1062.
(22) Liu, J.; Rinzler, A. G.; Dai, H. J.; Hafner, J. H.; Bradley, R. K.; Boul, P. J.; Lu, A.; Iverson, T.; Shelimov, K.; Huffman, C. B.; Rodriguez-Macias, F.; Shon, Y. S.; Lee, T. R.; Colbert, D. T.; Smalley, R. E. *Science* **1998**, *280*, 1253–1256.

Scheme 1. Layer-by-Layer Assembled MWNT Thin Film with Positively and Negatively Charged MWNTs

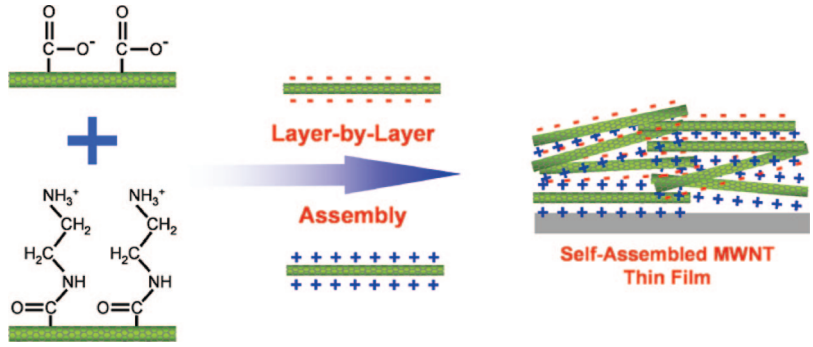

$\pi-\pi$ stacking interactions between the side wall and aromatic groups,[24−26] and polymer wrapping of nanotubes.[27−29]

One simple and versatile method to assemble dispersed CNTs into thin-films is using layer-by-layer (LBL) assembly,[30] which consists of the repeated, sequential immersion of a substrate into aqueous solutions of complementarily functionalized materials. This technique can produce conformal ultrathin films and highly tunable surfaces using various nanomaterials on geometric surfaces. Recently, electrostatic layer-by-layer (LBL) assembly in which CNTs have been alternated with polymers[7,31,32] for various energy storage and conversion devices been shown to exhibit improved networks for electrochemical energy applications relative to conventional electrodes,[7,31,32] and increased mechanical strength by preventing phase separation and realizing uniform nanoscale blends.[5,33]

In this work, we show, for the first time, the preparation of all MWNT thin films based on the LBL assembly method. Multiwall nanotubes (MWNTs) chemically modified to exhibit acid and base groups can be treated much like weak polyelectrolytes with precisely controlled thickness. The LBL assembled thin films of weak polyelectrolytes such as poly(acrylic acid) or poly(allylamine hydrochoride) exhibit tunable thickness, composition ratio, and porosity by controlling the degree of ionization of polyelectrolytes with the pH of the assembly solution, which ultimately affects chain conformation within the film and film morphology.[34−36] Negatively and positively charged MWNTs have been functionalized on their exterior walls with carboxylic acid groups[23,37] yielding MWNT-COOH, and with amine groups[38,39] yielding MWNT-NH_2. LBL MWNT films, which consist of well-dispersed MWNTs, have been produced by LBL using stable dispersions of negatively and positively charged MWNTs (Scheme 1). Unlike other multilayer assemblies that contain CNTs as one of two or more components, these systems incorporate MWNTs without the incorporation of additional organic materials; this difference can enable the development of 100% CNT thin films with properties that can be manipulated using assembly conditions. In particular, the irregular shape of the CNTs enables the direct formation of porous, all-carbon nanostructures with high surface area. MWNT thin films show pH-dependent thickness and surface topology, which are characteristics of LBL thin films of weak polyelectrolytes. We demonstrate that the surface topology and the inner structure of MWNT thin films are interconnected random network structures with physical entanglements using atomic force microscopy (AFM), scanning electron microscopy (SEM), and swelling experiments. Sheet resistance and cyclic voltammetry measurements show that these MWNT thin films are promising electrode materials for high-power and high-energy electrochemical devices.

Experimental Section

Functionalization of Negatively and Positively Charged MWNTs. MWNTs prepared by a conventional CVD method were purchased from NANOLAB (95% purity, length 1−5 μm, outer diameter 15 $\pm$ 5 nm). MWNTs were refluxed in concentrated H_2SO_4/HNO_3 (3/1 v/v, 96% and 70%, respectively) at 70 °C to prepare carboxylic acid functionalized MWNTs (MWNT-COOH), and then washed with deionized Milli-Q water (18 MΩ·cm) water several times using nylon membrane filter (0.2 μm). Dried carboxylated MWNTs were chlorinated by refluxing for 12 h with $SOCl_2$ (Sigma-Aldrich) at 70 °C. After evaporating any remaining $SOCl_2$, amine functionalized MWNTs (MWNT-NH_2) were obtained by reaction with $NH_2(CH_2)_2NH_2$ (Sigma-Aldrich) in dehydrated toluene (Aldrich) for 24 h at 70 °C. After washing with ethanol and deionized water several times, MWNT-NH_2 powder was obtained from drying at 50 °C in vacuum for 24 h.

Layer-by-Layer Assembly of MWNT Thin Films. Dried MWNT-COOH and MWNT-NH_2 powders were sonicated using a Branson Bransonic 3510 ultrasonic cleaner (40 kHz) in Milli-Q water (18 MΩ·cm) for several hours to form stable dispersions. These solutions were subjected to dialysis against Milli-Q water

(23) Esumi, K.; Ishigami, M.; Nakajima, A.; Sawada, K.; Honda, H. *Carbon* **1996**, *34*, 279–281.
(24) Chen, R. J.; Zhang, Y. G.; Wang, D. W.; Dai, H. J. *J. Am. Chem. Soc.* **2001**, *123*, 3838–3839.
(25) Nakashima, N.; Tomonari, Y.; Murakami, H. *Chem. Lett.* **2002**, 638–639.
(26) Paloniemi, H.; Lukkarinen, M.; Aaritalo, T.; Areva, S.; Leiro, J.; Heinonen, M.; Haapakka, K.; Lukkari, J. *Langmuir* **2006**, *22*, 74–83.
(27) O'Connell, M. J.; Boul, P.; Ericson, L. M.; Huffman, C.; Wang, Y. H.; Haroz, E.; Kuper, C.; Tour, J.; Ausman, K. D.; Smalley, R. E. *Chem. Phys. Lett.* **2001**, *342*, 265–271.
(28) Liu, P. *Eur. Polym. J.* **2005**, *41*, 2693–2703.
(29) Satake, A.; Miyajima, Y.; Kobuke, Y. *Chem. Mater.* **2005**, *17*, 716–724.
(30) Decher, G. *Science* **1997**, *277*, 1232–1237.
(31) Zhang, M. N.; Yan, Y. M.; Gong, K. P.; Mao, L. Q.; Guo, Z. X.; Chen, Y. *Langmuir* **2004**, *20*, 8781–8785.
(32) Zhang, M. N.; Su, L.; Mao, L. Q. *Carbon* **2006**, *44*, 276–283.
(33) Olek, M.; Ostrander, J.; Jurga, S.; Mohwald, H.; Kotov, N.; Kempa, K.; Giersig, M. *Nano Lett.* **2004**, *4*, 1889–1895.
(34) Shiratori, S. S.; Rubner, M. F. *Macromolecules* **2000**, *33*, 4213–4219.
(35) Choi, J.; Rubner, M. F. *Macromolecules* **2005**, *38*, 116–124.
(36) Mendelsohn, J. D.; Barrett, C. J.; Chan, V. V.; Pal, A. J.; Mayes, A. M.; Rubner, M. F. *Langmuir* **2000**, *16*, 5017–5023.
(37) Chen, J.; Hamon, M. A.; Hu, H.; Chen, Y. S.; Rao, A. M.; Eklund, P. C.; Haddon, R. C. *Science* **1998**, *282*, 95–98.
(38) Baker, S. E.; Cai, W.; Lasseter, T. L.; Weidkamp, K. P.; Hamers, R. J. *Nano Lett.* **2002**, *2*, 1413–1417.
(39) Ramanathan, T.; Fisher, F. T.; Ruoff, R. S.; Brinson, L. C. *Chem. Mater.* **2005**, *17*, 1290–1295.

for several days to remove any byproduct and residual during functionalization. The concentrations (0.5 mg/ml) and pHs of solutions were precisely adjusted after dialysis, and resulting solutions were sonicated briefly prior to LBL assembly. MWNT films were fabricated with a modified Carl Zeiss DS50 programmable slide stainer on various substrates. Substrates were first dipped into a MWNT-NH_2 solution for 30 min, then three baths of Milli-Q water for 2, 1, 1 min each. The substrates were then exposed to a MWNT-COOH solution for 30 min, and washed in three baths of Milli-Q water for 2, 1, 1 min each. This cycle makes one bilayer of MWNT-NH_2 and MWNT-COOH, denoted (MWNT-NH_2/MWNT-COOH). The cycle was repeated to reach the desired number of bilayers of MWNT thin films. To exclude the effect of gradual precipitation of MWNTs in the solutions after long timeframes (several days), a disk magnetic stirrer (VWR International) under the dipping bath was installed, which allowed the circulation of MWNT solution upon layering on the substrate and thus rendered uniform and high quality MWNT thin films on the substrate.

Characterization. The surface chemistry of functionalized MWNTs was analyzed using a Kratos AXIS Ultra Imaging X-ray photoelectron spectrometer (XPS). All spectra were calibrated with the C 1s photoemission peak for sp^2 hybridized carbons at 284.5 eV. Curve fitting of the photoemission spectra was done after a Shirley type background subtraction. The zeta potential as a function of pH was measured using a Zeta PALS ((Brookhaven Instrument Corp.) to determine the effect of surface charge on MWNT dispersions. Thickness of MWNT thin films on silicone wafers was determined using a Tencor P-10 profilometer. Surface topology of MWNT thin films was examined using an AFM microscope (Digital Instruments EnviroScope, Veeco) in the tapping mode in the air. The root-mean-square (rms) roughness of the LBL films was examined from AFM images with a size of $4 \times 4\ \mu m^2$. Surface morphology and interior structure of MWNT thin films were investigated using a scanning electron microscope (JEOL 6320 SEM) operating at 3.0 and 5.0 kV. Refractive indices of MWNT thin films were determined using a J.A.Woolham Co. VASE spectroscopic ellipsometer, and data fitting was performed with a Cauchy model using the WVASE32 software package. Sheet resistances were measured for films deposited on glass slides by using a standard four-point probe configuration (Signatone model S-302−4). A series of 3−4 measurements were taken on each film, and the measurements then were averaged to give the final reported value with the standard deviation as an error range. A three-electrode cell was employed for electrochemical measurements, where a saturated calomel electrode (SCE) (Analytical Sensor, Inc.) and Pt wire were used as the reference and counter electrodes, respectively. MWNT thin films on ITO coated glass slides were used as the working electrode. Cyclic voltammetry was performed between −0.25 and 0.80 V (SCE) at room temperature in 1.0 M H_2SO_4 solution using a bipotentiostat (PINE instrument).

Results and Discussion

To introduce MWNTs into an electrostatic LBL system, negatively and positively charged MWNTs were created via chemical functionalization of exterior surfaces. Negatively charged MWNTs were prepared by oxidation with extremely aggressive acids, which could render oxygen-containing groups such as carboxylic acid groups on the MWNT surface (MWNT-COOH).[23,37] Carboxylic acid groups (COOH) on the surface of MWNTs exist as carboxylate anions (COO^-) in aqueous solution, yielding negatively charged MWNTs, (MWNT-COOH). Positively charged MWNTs were prepared by introducing amine groups (NH_2),[38,39] which could be protonated over a broad pH range, through the formation of amide bonds with COOH functionalized MWNTs and excess ethylene diamine.

XPS Results of Surface Functionalized MWNTs. X-ray photoemission spectroscopy (XPS) elemental analysis was performed to probe the surface functional groups on the modified MWNTs, as shown in Figure 1a. The O_{1s} photoemission peak was clearly observed on COOH functionalized MWNTs and amine functionalized MWNTs. The amount of surface oxygen-containing functional groups was found to increase with longer oxidation time, as indicated by the increase in the O_{1s} peak intensity from oxidation time from 1 to 2 h. The XPS analysis of C_{1s} spectra (Figure 1b−e) show detailed surface functional groups on the MWNTs. An asymmetric peak from sp^2 hybridized carbons centered at 284.5 eV with an extended tail at the higher energy region[40] was generated for raw MWNTs, and the same form of the asymmetric peak was used for all other fittings of the sp^2 hybridized graphite-like carbons. Using this asymmetric peak as a reference, the C_{1s} peak of the oxidized MWNTs was fitted to five Gaussian−Lorentzian shape peaks, which were attributed to sp^3 hybridized diamond-like carbons (285.2 ± 0.1 eV), C−O (286.2 ± 0.1 eV), carbonyls C═O (286.8 ± 0.2 eV), hydroxyls C-OH (287.5 ± 0.1 eV), and carboxyls O═C-OH (288.9 ± 0.2 eV).[41] The intensities of these peaks increased relative to sp^2 hybridized graphite-like carbons with oxidation time (Figures 1b and 1c). After 2 h of oxidation, the MWNT-COOH produced stable dispersions in water as a result of electrostatic repulsion between MWNTs (Figure S2a, Supporting Information). In the case of the 1 h oxidation MWNTs, a stable dispersion in water was not obtained, which could be the result

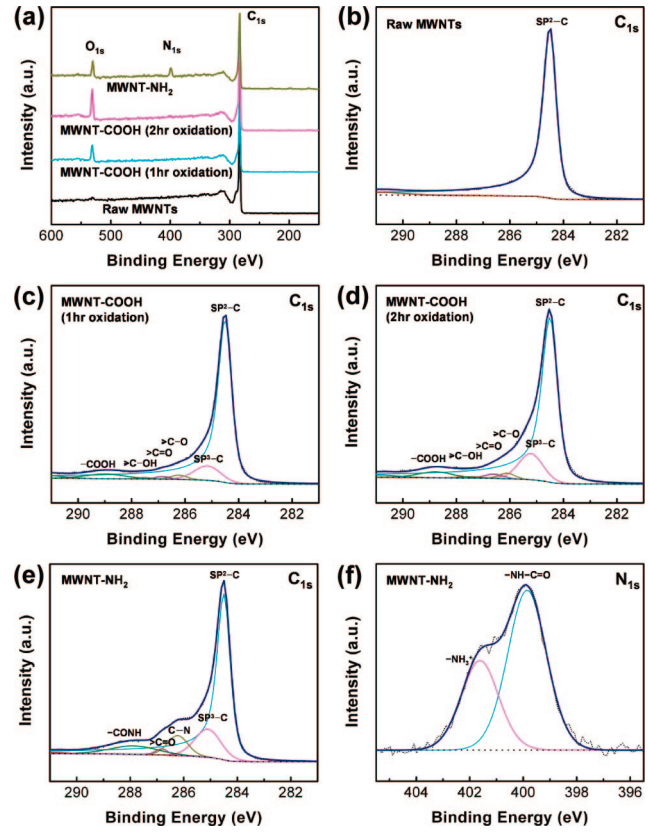

Figure 1. X-ray photoelectron spectroscopy (XPS) spectra of functionalized MWNTs. (a) Wide scan survey, (b) raw MWNTs C_{1s} spectra, (c) MWNT-COOH (1 h oxidation) C_{1s} spectra, (d) MWNT-COOH (2 h oxidation) C_{1s} spectra, (e) MWNT-NH_2 C_{1s} spectra, (f) MWNT-NH_2 N_{1s} spectra.

(40) Ago, H.; Kugler, T.; Cacialli, F.; Salaneck, W. R.; Shaffer, M. S. P.; Windle, A. H.; Friend, R. H. *J. Phys. Chem. B* **1999**, *103*, 8116–8121.
(41) Murphy, H.; Papakonstantinou, P.; Okpalugo, T. I. T. *J. Vac. Sci. Technol., B* **2006**, *24*, 715–720.

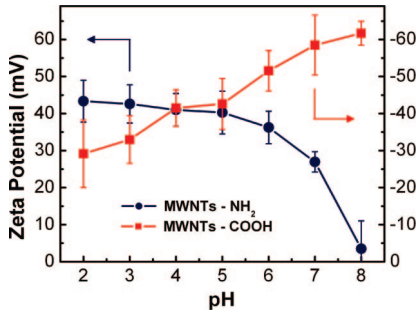

Figure 2. pH-dependent zeta potential of functionalized MWNTs. Each point of zeta potential value was obtained by more than 10 measurements and error bars show standard deviations.

of insufficient negative charges to prevent aggregation and gravitational precipitation of MWNTs due to van der Waals interaction between MWNTs. The XPS analysis of C_{1s} and N_{1s} of MWNT-NH_2 (Figures 1e and f) suggests the presence of amide bonds N−C═O (287.9 eV in C_{1s} and 399.9 ± 0.1 eV in N_{1s}), and amines NH_2 (NH_3^+) (286.2 eV in C_{1s} and 401.8 ± 0.2 eV in N_{1s}),[39] which indicate successful introduction of primary amine groups via the formation of amide bonds. Examples of the MWNT solutions used for LBL assembly are also pictured in Figure S2b (Supporting Information). The pH of MWNT-COOH (0.5 mg/ml) and MWNT-NH_2 (0.5 mg/mL) solutions were adjusted to pH 3.5 and 2.5 respectively after dialysis. The solutions remained clearly dispersed even after one month following pH adjustment, suggesting that stable dispersions were achieved in the MWNT solutions. No precipitation of MWNTs was observed in the case of the MWNT-COOH solution, but some precipitation was noted for concentrated MWNT-NH_2 solutions in the bottom of the glass vial after several days. This suggests that the precipitation rate of positively charged MWNTs is much faster than negatively charged ones due to weak electrostatic repulsion between the MWNTs-NH_2.

Surface Charge and LBL Assembly of Functionalized MWNTs. The surface charges on MWNTs are not only key to creating stable colloidal dispersions, but are also required elements to achieving LBL assembled films. As shown in Figure 2, the zeta potential of the MWNT-COOH was found to decrease with decreasing pH due to the protonation of the COOH group on the MWNTs. On the other hand, the zeta potential of MWNT-NH_2 decreased as the pH was increased due to changes in the degree of ionization of the NH_2 group on MWNTs. This behavior is very similar to weak polyelectrolytes such as poly(acrylic acid) (PAA) and poly(allylamine hydrochloride) (PAH).[34] An interesting difference between PAA and MWNT-COOH is the difference in the degree of ionization observed at low pH. The degree of ionization of the PAA solution approaches zero,[35] but MWNT-COOH still has enough negative charge to maintain stable dispersions at pH 2 (approximately −30 mV). We speculate this difference comes from the different backbone structures to which the COOH groups are attached. The sp^2 hybridization character of the MWNT backbone can yield a much lower pK_a (pK_a of benzoic acid:[42] 4.19)compared to that of PAA (pK_a of propanoic acid:[42] 4.86), allowing higher degrees of ionization at lower pH. Therefore, it is postulated that MWNTs can be directly incorporated into multilayer films by electrostatic interactions (Scheme 1), and the thickness and morphology of the resulting LBL films can be controlled like weak polyelectrolytes by altering the assembly pH values.

Figure 3a shows the thickness of MWNT thin films at various pH conditions as a function of the number of bilayers. Figure 3b summarizes the averaged bilayer thickness for films assembled as a function of MWNT-COOH pH. Figure 3c shows representative optical images of MWNT thin films on Si wafer from pH 2.5 (+)/4.5 (−), where each film has a characteristic reflective color corresponding to its thickness. The films darken with increasing thickness and appear black at a thickness greater than 300nm. For convenience of comparison, MWNT films assembled from MWNT-NH_2 at pH 2.5 and MWNT-COOH at pH 3.5 will be denoted as pH 2.5 (+)/3.5 (−). The pH of MWNT-COOH was varied from 2.5 to 4.5 while fixing the pH of MWNT-NH_2 at 2.5 so as to maintain sufficient positive surface charge. The thickness per bilayer of the MWNTs films increases as the pH of the MWNT-COOH solution is decreased (Figure 3b). This increase in thickness from pH 4.5 to 2.5 is likely due to the significant charge decrease of carboxylic acid functionalized MWNTs from pH 4.5 to pH 2.5 as was proven by zeta potential measurements (Figure 2). The lowered degree of ionization on the nanotubes may require more adsorption of the negatively charged MWNTs to balance the positive charge for each bilayer. Interestingly, weak polyions show similar behavior in layer-by-layer assembly,[34,43] with bilayer thicknesses increasing when the degree of ionization of one of the polyelectrolytes is lowered; however, the behavior in weak polyions is due to changes in the conformation of polyelectrolyte chains from flat adsorbed coils to thick looped structures on the top surface. The rigidity of carbon nanotubes would preclude such changes in nanotube conformation on a molecular level; however, there may be differences in the degree of interpenetration between deposited nanotubes based on the nanotube charge density. The presence of fixed charges along the MWNT surface is influenced by the acid−base equilibria of the acid and amine groups, leading to strong charge regulation and an effective pK_a that impacts shielding effects; however additional effects due to Van der Waals interactions, excluded volume, and osmotic effects may also be important, as predicted theoretically for charged adsorbed layers.[44] In this case, one would anticipate higher degrees of nanotube interpenetration with increasing tube charge density, which could also lead to thinner films with somewhat denser packing between nanotubes. Finally, high charge densities may cause the nanotubes to adsorb in a slightly more flattened arrangement on the oppositely charged surface due to electrostatic forces, leading to thinner interpenetrated structures.

Microstructure of LBL Assembled, Surface Functionalized MWNT Thin Films. Figure 4 shows tapping-mode AFM images of MWNT thin films assembled at different pH conditions with increasing number of bilayers. All AFM images clearly show that MWNT thin films have an interconnected network structure with separated individual MWNTs, which have an average diameter of 15 ± 5 nm. Root-mean-squared (rms) roughness increases with the number of bilayers, showing similar behavior for different pH conditions at the beginning stages. However, assembly from pH 2.5 (+)/2.5 (−) shows a steep increase of rms roughness from 9 bilayers to 15 bilayers compared to other

(42) *CRC Handbook of Chemistry and Physics*, 79th ed.; CRC Press: Boca Raton, FL, 1998.
(43) Tagliazucchi, M.; Williams, F. J.; Calvo, E. J. *J. Phys. Chem. B* **2007**, *111*, 8105–8113.
(44) Tagliazucchi, M.; Calvo, E. J.; Szleifer, I. *J. Phys. Chem. C* **2008**, *112*, 458–471.

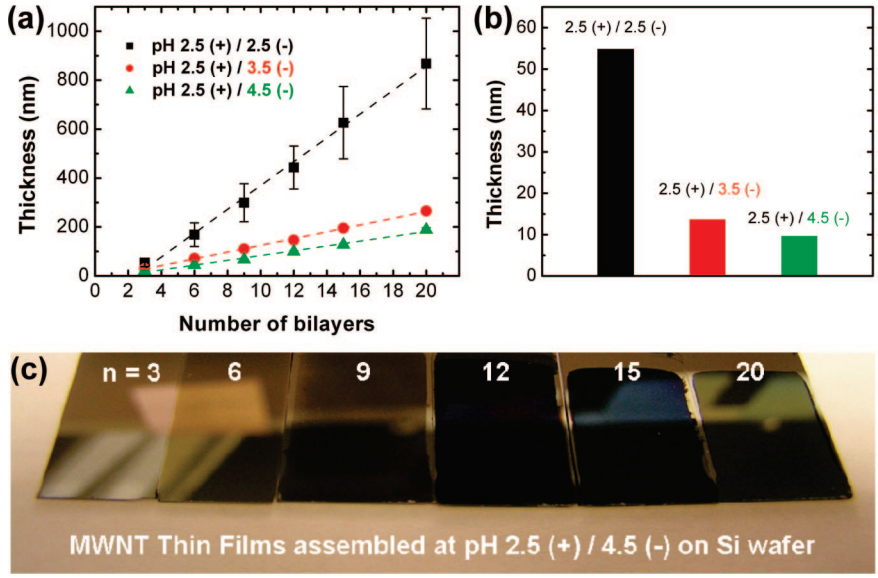

Figure 3. (a) Thickness of MWNT thin films under varying assembly pH conditions. The dashed lines are linear fit with standard deviations as error bars. pH 2.5 (+)/2.5 (−) indicates MWNT thin films assembled from MWNT-NH_2 at pH 2.5 and MWNT-COOH at pH 2.5. (b) pH dependent average bilayer thicknesses. (c) Representative digital picture image of assembled MWNT thin films on Si wafer from pH 2.5 (+)/4.5 (−). Number on image indicates the number of bilayer (n) in (MWNT-NH_2/MWNT-COOH)$_n$.

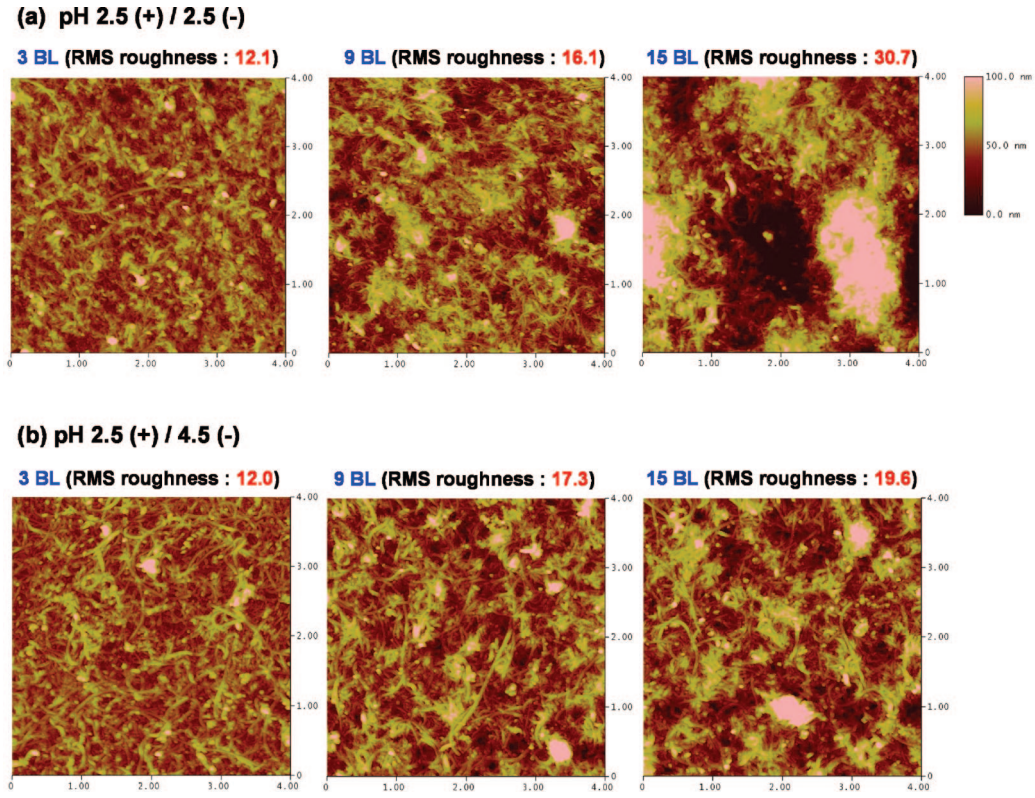

Figure 4. Atomic force microscopy (AFM) height images of (MWNT-NH_2/MWNT-COOH)n thin films deposited at different pH conditions. (a) pH 2.5 (+)/2.5 (−), (b) pH 2.5 (+)/4.5 (−). Size of each image is 4 μm × 4 μm.

pH conditions. Images of pH 2.5 (+)/3.5 (−) condition were not shown because of the resemblance of topography with the pH 2.5 (+)/4.5 (−) condition. The higher roughness for the pH 2.5(−) films can be explained by the higher thickness of the films and the fact that the lowered surface charge density of the MWNT-COOH at pH 2.5 may lead to the looser adsorption of larger numbers of MWNTs, as discussed above, resulting in rougher surfaces, while the other two assemblies at higher MWNT-COOH pH show relatively uniform and somewhat more densely packed MWNT network structures.

The porous network structure of the LBL assembled MWNT thin films can be contrasted with simple cast films of raw MWNTs. Figure 5 shows comparison SEM top view images of a cast film using raw MWNTs solution after 2 h of sonication and a 20 bilayers MWNT thin film assembled at pH 2.5 (+)/2.5 (−). The cast film of raw MWNTs shows aggregation and

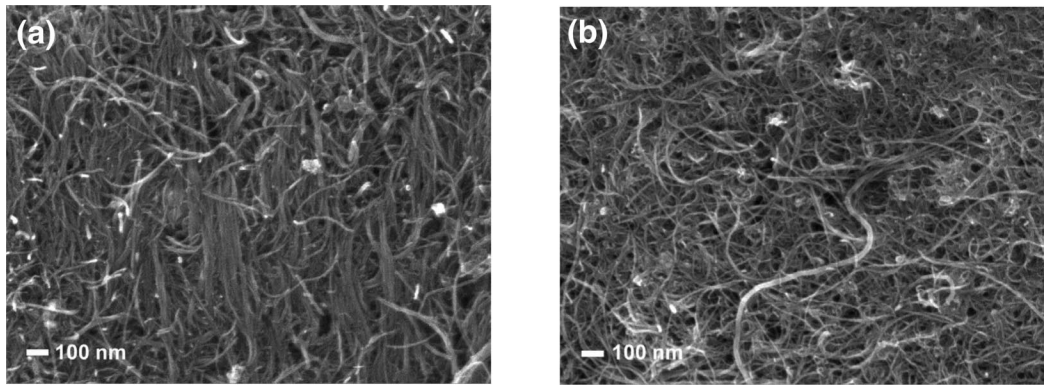

Figure 5. Comparison of the topology of MWNTs using scanning electron microscopy (SEM) images. (a) Deposition of raw MWNT solution on silicone wafer after 2 h sonication. (b) LBL assembled MWNT thin film at (pH 2.5 (+)/2.5 (−))$_{20}$.

alignment of bundles of MWNTs due to van der Waals interactions and capillary forces. These films exhibit weak mechanical integrity, poor control of thickness and dense packing, leading to diminishment of the available surface area of the MWNTs. On the other hand, the LBL assembled MWNT films yield randomly oriented individual MWNTs with well developed nanoscale pores, making MWNT thin films an ideal electrode structure with mixed ionic/electronic conducting channels. These differences come from the electrostatic repulsion between nanotubes that act against van der Waals interactions that yield close packed aggregates, as well as the electrostatic cross-linking between positively and negatively charge MWNTs during the LBL process that lead to randomly oriented, kinetically driven CNT arrangements in the film. A cross-sectional view of a MWNT thin film (Figure 6a) demonstrates the conformal and uniform nature of the coating generated with LBL of MWNTs on silicon wafer, suggesting their application to substrates without any geometric constraint. A torn film shown in the Figure 6a insert reveals that most of the MWNTs in the film are not parallel with the substrate, but form an interpenetrated structure with random orientations of the nanotubes. An angled cross-sectional view was created by cutting films on a slant (Figure 6b); it more clearly shows the internal structure of the film, proving that a highly interpenetrated and porous structure is created. Since the MWNTs have intrinsically high electrical conductivity and higher surface area, these porous network structures can work as fast electronic and ionic conducting channels, providing the basis for design of the ideal matrix structure for energy conversion as well as energy storage devices.

To measure the porosity of MWNT thin films, we used a recently developed model[45] by Lee and co-workers with ellipsometry, which allows the estimation of porosity from the refractive indices of materials in two different medium. MWNT thin films were cross-linked by amide bond formation by heat-treatment at 150 °C in vacuum, and the refractive index was measured in air and ethanol. To estimate the porosity we used the equation (eq S2, Supporting Information) derived from the most frequently used Lorentz−Lorentz mixing rule of refractive index (eq S1, Supporting Information). The estimated porosity range is about 35−43% depending on the sample and its thickness. Figure S4 (Supporting Information) shows representative refractive indices values in air and ethanol and the estimated porosity of MWNT thin films assembled at pH 2.5 (+)/4.5 (−). There was some difficulty in measuring the refractive index accurately for the thicker samples assembled at lower pH, especially at pH 2.5 (+)/2.5 (−) due to high surface roughnesses and absorption, making it difficult to determine the optical constant of thin films using spectroscopic ellipsometry.[46]

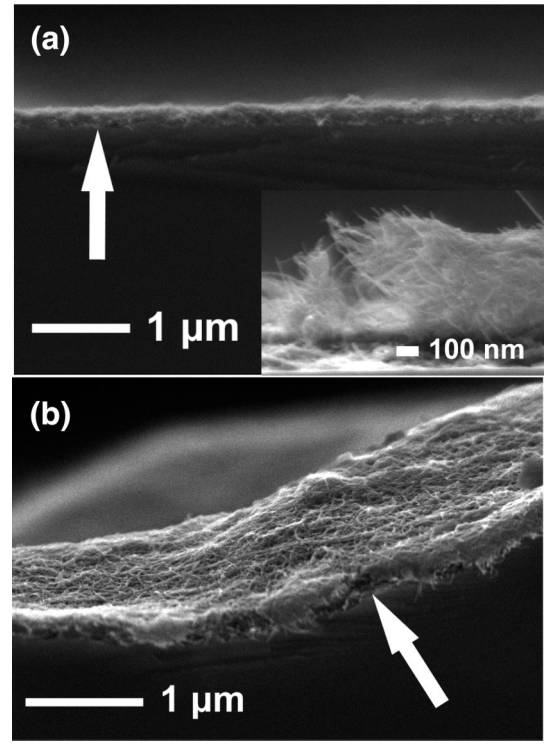

Figure 6. Scanning electron microscopy (SEM) images of MWNT thin films. (a) A cross-section view of 15 bilayers of MWNT film (pH 2.5 (+)/3.5 (−)), and (b) a titled cross-sectional view of a 20 bilayer MWNT film (pH 2.5 (+)/4.5 (−)). White arrows indicate the interface between silicone substrate and MWNT thin films.

Swelling Behavior and Mechanical Integrity of LBL Assembled, Surface Functionalized MWNT Thin Films. The time-dependent swelling behavior of the MWNT thin film in water was systematically investigated. When the thin film (156 ± 6 nm) was assembled at pH 2.5 (+)/4.5 (−) on Si substrate was immersed in deionized water, small blisters were formed immediately in the center region of the film, then quickly grew and coalesced to large blisters which reached the boundary of substrate (Figure 7a−d). There is electrostatic repulsion between

(45) Lee, D.; Rubner, M. F.; Cohen, R. E. *Nano Lett.* **2006**, *6*, 2305–2312.

(46) Tompkins, H. G. I.; Eugene, A. *A Handbook of Ellipsometry*; William Andrew Publishing: New York, 2005.

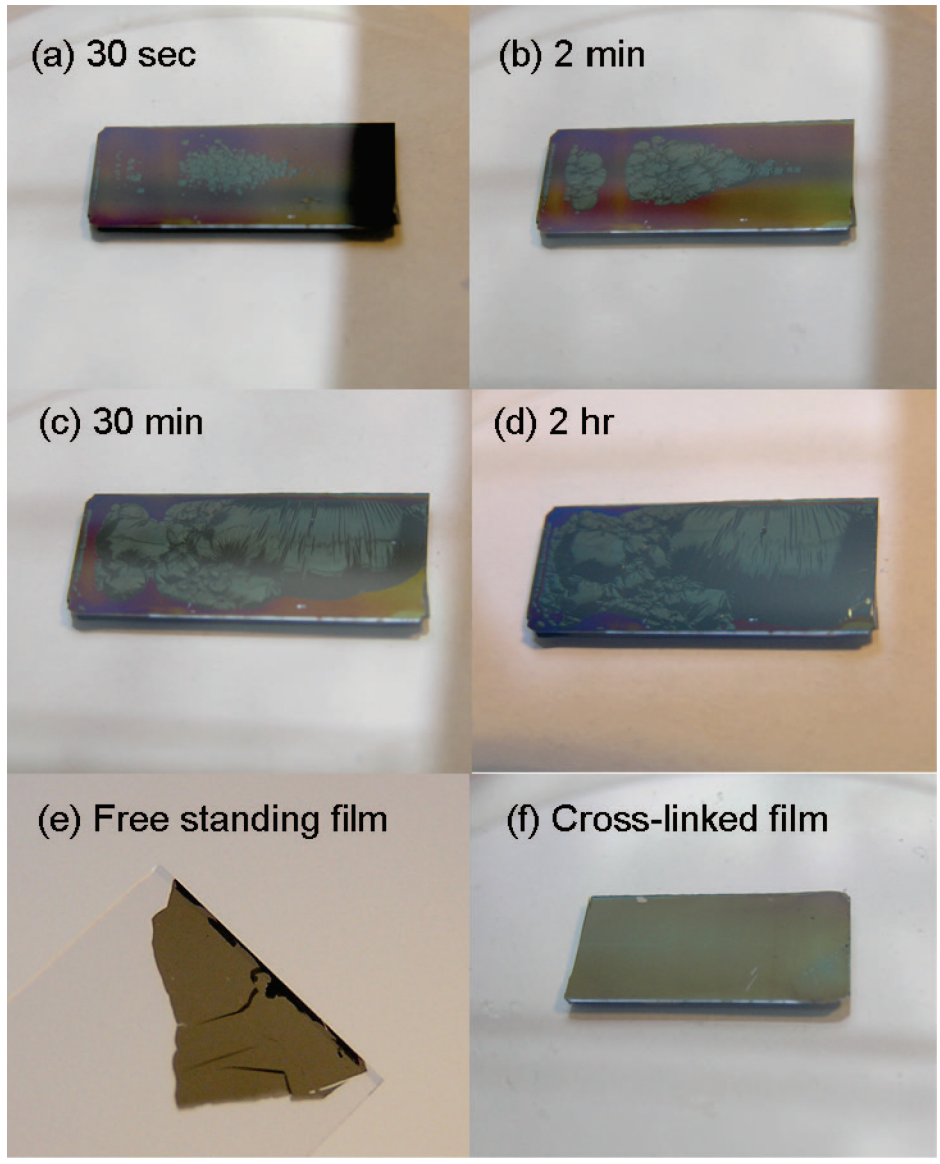

Figure 7. (a−d) Time-dependent water swelling behavior of MWNT thin film assembled at pH 2.5/4.5. (e) Free-standing film collected on a glass slide tip. (f) Thermally cross-linked film immersed after 24 h in water. Note the structural integrity is maintained after cross-linking of the MWNT film at 150 °C in vacuum during overnight.

the negatively charged MWNTs in the film due to charge imbalances induced by a decrease in the degree of ionization of NH_2 (NH_3^+) groups, and increase of COOH (COO^-) groups in the water (pH 6.0), causing the film to swell. When the film is supported on a substrate and swollen in water, then the film can expand freely in the thickness direction, but it is confined laterally, creating strain in the lateral direction. Unlike polyelectrolyte-containing LBL films, rigid MWNT films cannot undergo high elastic strain to compensate for this stress. As a result, the generation of blisters and delamination of the film from the substrate begins from the point which has a larger strain energy compared to the adhesion energy between film and substrate to release excess strain energy in the film. Although individual MWNTs are quite elastic (bending modulus is about 30 GPa[47]),[48] they cannot change their molecular conformations as polymers can due to rigidity; however, physical entanglements between nanotubes exist in the films due to their large aspect ratio and sinuous structure, allowing the film to maintain its mechanical integrity in spite of the detachment from the substrate (Figure 7d). This physical detachment from the substrate and expansion of the films via rearrangements of MWNTs in the film could be a mechanism of releasing strain energy in the film.[49] Gentle shaking of the substrate lead to the isolation of free-standing MWNT films due to their weak mechanical integrity. Part of the free-standing MWNT film was scooped from the water on a glass slide, and while maintaining the integrity of the film (Figure 7e). To increase the mechanical strength of the film and its adhesion to the substrate, thermally induced cross-linking (150 °C in vacuum) of the MWNT thin film was conducted, which created amide bonds between the NH_3^+ and COO^- groups. XPS peaks of N_{1s} region (Figure S5, Supporting Information) showed a significant decrease in the

(47) Ciocan, R.; Gaillard, J.; Skove, M. J.; Rao, A. M. *Nano Lett.* **2005**, *5*, 2389–2393.
(48) Bernholc, J.; Brenner, D.; Nardelli, M. B.; Meunier, V.; Roland, C. *Ann. Rev. Mater. Res.* **2002**, *32*, 347–375.
(49) Sharp, J. S.; Jones, R. A. L. *Phys. Rev. E* **2002**, *66*, 011801.

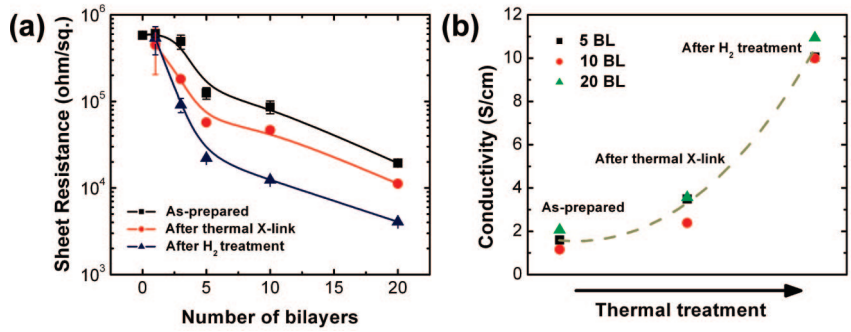

Figure 8. (a) Sheet resistance of the MWNT thin films. (■) as-assembled MWNT thin films assembled at pH 2.5 (+)/3.5 (−). (●) MWNT films after a thermal treatment at 150 °C in vacuum during overnight. (▲) MWNT films after a second heat-treatment at 300 °C in H_2 for 2 h. (b) Corresponding electrical conductivity of the MWNT thin films in S/cm obtained from the data in (a), electrode thickness and area.

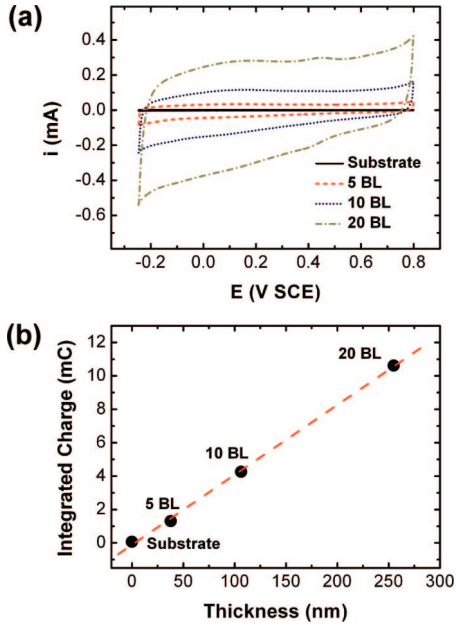

Figure 9. (a) Cyclic voltammograms obtained from MWNT thin films on ITO-coated glass electrode (after the second heat-treatment) in 1.0 M H_2SO_4 at room temperature. A scan rate of 50 mV/s was used. (b) Integrated charge from cyclic voltammograms vs thickness of film measured from profilometer.

ammonium peak after the heat-treatment, which indicates the formation of amide bonds from charged ammonium groups.[50] Figure 7f shows that this cross-linked MWNT thin film is intact in water, which does not undergo swelling and preserves its original shape. Thus, thermal cross-linking of the MWNT films not only prevents swelling from electrolytes, but also provides mechanical strength and prevents lift-off and delamination from the substrate, which are required properties for real applications as electrodes for energy devices.

Electrochemical Properties of LBL Assembled, Surface Functionalized MWNT Thin Films. The sheet resistance of the MWNTs thin films assembled at pH 2.5 (+)/3.5 (−) on a glass substrate was measured by a 4-point probe as a function of the number of bilayers (Figure 8). The sheet resistance of as-prepared samples exhibit high values, thought to be due to the disruption of the conjugated carbon sp^2 orbitals on the MWNT exterior surface with the formation of surface functional groups.

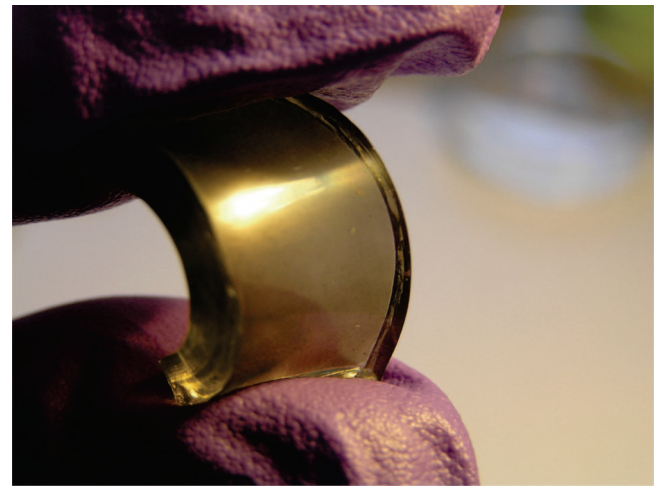

Figure 10. Optical image of a MWNT thin film of 10 bilayers assembled at pH 2.5 (+)/3.5 (−) on PAH coated PDMS substrate.

The sheet resistance of LBL MWNT samples was shown to decrease with increasing numbers of bilayers, suggesting that the conductivity of the thin films increases with added layers. This effect may be attributed to denser packing and more continuous intercolated pathways for electron transport in the thicker films. The heat-treatment at 150 °C in vacuum decreased the sheet resistance of LBL MWNT thin films roughly by one-half, which could be attributed to facilitated electron flow between adjacent MWNTs cross-linked via amide formation. A subsequent heat-treatment at 300 °C in hydrogen atmosphere for 2 h was used to burn off residual surface functional groups on the MWNTs, enabling direct contact was achieved between the electronically conducting MWNTs. This process led to a further decrease in the sheet resistance of the MWNT thin film, showing an average of an 82% reduction compared with as-assembled samples, as well as a film thickness that was slightly reduced by about 10%. Further increases in electrical conductivity may be possible by higher temperature heat-treatments. To compare with other CNT electrodes reported previously, the all MWNT LBL electrodes were found to have sheet resistivity on the order of ~0.1 Ωcm (~10 S/cm) after heat treatments. Although this resistivity is higher than those of vertically oriented SWNT electrodes[12] (0.01 Ωcm, without surface functionalization) and ultrathin conductive SWNT films (1.5×10^{-4} Ωcm),[51] it is considerably lower than SWNT polymer composite electrodes (1 Ωcm).[52] Also the electrical conductivity of all MWNT LBL electrodes (Figure 8b) after heat-treatments is comparable or slightly higher than similar functionalized

(50) Harris, J. J.; DeRose, P. M.; Bruening, M. L. *J. Am. Chem. Soc.* **1999**, *121*, 1978–1979.

MWNTs capacitor,[53] which showed electrical conductivity (2−8 S/cm) as function of oxidation time, and ~3 S/cm at highest capacitance (~60 F/g). The high conductivity of the LBL electrodes can be attributed to the binder-free, all carbon nanotube composition of the multilayer film and its unique, highly interconnected morphology. These results show that heat-treatments of MWNT thin films after LBL assembly can increase their electrical conductivity as well as their mechanical integrity (Figure 7).

Cyclic voltammograms of heat-treated MWNT thin films (0.7 cm × 2 cm) on ITO-coated glass assembled at pH 2.5 (+)/3.5 (−) were obtained in 1.0 M H_2SO_4 solution as a function of the number of bilayers (Figure 9a). The thickness dependent voltammetry curves showed considerably rectangular shapes, which is indicative of capacitive behavior of carbon materials.[14] Integrated surface charge from adsorbed and desorbed ions on MWNT thin film electrode was found to scale linearly as a function of film thickness (Figure 9b). An average capacitance of 132 ± 8 F/cm^3 (159 ± 10 F/g) was found and this value is considerably higher than those of vertically aligned CNTs[12] conventional CNT electrodes[14,53] as a result of the high CNT densities and well developed nanopores in the LBL MWNT thin films. This result indicates the potential to gain precise control of charge and energy storage in MWNT thin films by controlling the number of bilayers and film thickness in the LBL assembly.

Finally, to demonstrate the universality of the thin film application, a MWNT thin film was deposited on a flexible polydimethylsiloxane (PDMS) substrate. Figure 10 presents a 10 bilayer MWNT thin film assembled at pH 2.5 (+)/3.5 (−) on PAH coated PDMS. Because of the ultrathin thickness of the MWNT film, the coating remains conformal and well-adhered even on a highly deformed PDMS substrate. This interesting result shows the possibility to design flexible energy storage and conversion devices[19] utilizing LBL assembled MWNTs as electrodes, electrical circuits, and current collectors.

Conclusions

Novel all-MWNT assemblies have been created through the alternation of surface functionalized positively and negatively charged MWNTs using the layer-by-layer technique, MWNT thin film assemblies show resemblance to LBL assembly from conventional weak polyelectrolytes such as PAA and PAH, which allow control of thickness and morphology by adjusting their conformation in the film via the manipulation of assembly pH conditions. Although MWNTs cannot change their molecular level conformation with changes in the local charge density due to their intrinsic rigidity, the surface charge density of MWNTs could play an important role in controlling film thickness and roughness by adjusting the charge reversal mechanism as well as the degree of interpenetration. Interpenetrating MWNTs in the assembly make networks that can achieve high electronic conductivity, and the well-developed porous structures between the MWNTs may create fast ion diffusion channels to facilitate ion transport. The potential to achieve high capacitance in the MWNT thin films with precisely controlled capacity using LBL makes these MWNTs assemblies promising for supercapacitor electrodes. Capacitor performance tests including galvanostatic charge/discharge measurements and cycling tests are ongoing with various substrates and electrolytes for supercapacitor applications. We believe that these novel MWNT thin films fully utilize both advantages of intrinsic superior properties of functionalized MWNTs and precise control of the LBL system can be used to design ideal electrode materials for fuel cells, photoelectrochemical cells, batteries, supercapacitors, and gas and biosensors.

Acknowledgment. We acknowledge the Dupont-MIT Alliance for funding support of this project. This work made use of the Shared Experimental Facilities supported by the MRSEC Program of the National Science Foundation under award number DMR 02-13282. YSH thanks the support of Office of Naval Research under award number N000140410400. S.W.L. acknowledges a Samsung Scholarship from the Samsung Foundation of Culture.

Supporting Information Available: Synthesis scheme of (a) COOH and (b) NH_2 functionalized MWNTs, optical images functionalized MWNT solutions, representative atomic force microscopy (AFM) phase image of a MWNT thin film, representative refractive indexes of MWNT thin films to determine porosity, and XPS spectra of the N1s region of a MWNT film before and after heating. This material is available free of charge via the Internet at http://pubs.acs.org.

JA807059K

(51) Wu, Z. C.; Chen, Z. H.; Du, X.; Logan, J. M.; Sippel, J.; Nikolou, M.; Kamaras, K.; Reynolds, J. R.; Tanner, D. B.; Hebard, A. F.; Rinzler, A. G. *Science* **2004**, *305*, 1273–1276.
(52) Sung, J.; Jo, P. S.; Shin, H.; Huh, J.; Min, B. G.; Kim, D. H.; Park, C. *Adv. Mater.* **2008**, *20*, 1505–1510.
(53) Kim, Y. T.; Mitani, T. *J. Power Sources* **2006**, *158*, 1517–1522.